Asian Journal of Chemistry; Vol. 35, No. 12 (2023), 3093-3104

ASIAN JOURNAL OF CHEMISTRY

https://doi.org/10.14233/ajchem.2023.30738

Exploring Self-Assembled Cationic Nanostructures of Amphiphilic β-Peptides for Amplifying Drug Delivery Efficiency

R. GOEL[1,2,3,*], M. MANGAL[2], A. SHARMA[1], P. KUMAR[3] and A. GUPTA[4]

[1]Department of Chemistry, JECRC University, Ramchandpura, Sitapura Extension, Jaipur-303905, India
[2]Department of Chemistry, Poddar International College, Tagore Lane, Shipra Path, Mansarovar, Jaipur-302020, India
[3]CSIR-Institute of Genomics and Integrative Biology, Delhi University Campus, Mall Road, Delhi-110007, India
[4]Department of Chemistry, Dyal Singh College, University of Delhi, Lodhi Road, New Delhi-110003, India

*Corresponding author: E-mail: goel.rahul07@gmail.com

Received: 18 October 2023; *Accepted*: 13 November 2023; *Published online*: 2 December 2023; AJC-21474

In this study, a set of short sequences of amphiphilic peptides composed of synthetic amino acids β-alanine and ornithine were designed. The synthesis of these peptides was carried out in a solution phase and then self-assembled into cationic nanostructures. The formation of cationic nanostructures was confirmed using dynamic light scattering (DLS) and the morphology of the nanostructures was studied using transmission electron microscopy (TEM), which revealed that the nanostructure adopted a spherical shape. To gain insight into the conformation of both solid samples and peptide solutions, the Fourier transform infrared (FTIR) and circular dichroism (CD) spectroscopic analysis were performed. Furthermore, the ability of these nanostructures to encapsulate hydrophobic drugs were also investigated. Three different drugs were tested as model drugs: L-dopa, an anti-Parkinson's drug; curcumin, anti-cancerous drug and tetrabenazine, anti-Huntington's drug. The nanostructures exhibited the capacity to encapsulate these drugs in varying ratios.

Keywords: β-Peptide, Amphiphilic foldamers, Self-assembly, Cationic nanostructures, Drug delivery systems.

INTRODUCTION

The study of self-assembly in the design and development of nanobiomaterials has been a major source of motivation for scientists [1]. Synthetic peptidic systems have been particularly explored due to their compatibility with biological models. While earlier studies focused on the α-amino acid oligomers, but recent research has highlighted the structural and functional properties of α/β-heterogeneous backbone peptidic foldamers. By incorporating both α- and β-amino acid residues, these peptidic foldamers with heterogenous backbones closely resemble natural peptidic systems in their physical properties. Synthetic peptidic systems exhibit additional characteristics that enable them to resist proteases, making them more durable [2,3]. β-Amino acids with their structural constraints, provide conformational stability to the peptides, while functional side chains contribute desired functional properties. The strategic incorporation of amino acids into non-natural peptidic systems expands the repertoire of α/β-mixed peptidic systems opening up possibilities for various applications [4-6].

In recent years, several synthetic peptidic systems have been developed for efficient drug delivery, focusing on overcoming barriers that hinder drug distribution within the human body. Examples of such barriers include the blood-brain-barrier (BBB), multidrug resistance (MDR), specific cell targeting and side effects caused by drug overload [7]. To address these challenges, the peptidomimetic approach has been employed, which involves the designing molecule that mimic the properties of peptides [8]. The ability to control the morphology of short peptide sequences makes them promising candidates for chemotherapy applications [9]. Additionally, nano-sized particles have been found to exhibit greater cellular uptake compared to larger microsized molecules, indicating that nano-sized systems can serve as effective transport and delivery vehicles [10].

Three widely recognized therapeutic drugs were selected as examples; yet, each of these drugs (Fig. 1) possesses some significant shortcomings. For example, (i) L-Dopa is a well-known and oldest anti-Parkinson's drug and due to its easier administration, better tolerance, low cost it is the most effective.

But in advanced Parkinson's disease it's efficacy is significantly reduced due to its competing metabolism, *i.e.* peripheral decarboxylation and enzymatic degradation, which causes low bioavailability in plasma levels. Hence, large doses of L-dopa are required for treatment in Parkinson's patients. As dopamine has low lipid solubility and also due to enzymatic degradation it is orally inactive it cannot be used as a drug. In this regard, significant efforts have been made but drawbacks of pharmacotherapeutic management still persist [11,12]. (ii) Curcumin is a phytomolecule with extensive biological activities including anti-cancerous properties. But its poor solubility and rapid metabolism limited its clinical applications. Acidic pH of stomach makes it unstable and alkaline pH degrades it before reaching to the blood stream while other constituents metabolized by the renal metabolism. Resulting, the optimum quantity of the curcumin may not reach the blood resulting in no/less therapeutic effect [13]. (iii) Tetrabenazine is a popular and the only US FDA approved anti-Huntington's drug. It was previously used as an antipsychotic drug but now primarily used in the symptomatic treatment of hyperkinetic disorders. Tetrabenazine is a depletor of monoamine neurotransmitters serotonin, nor-epinephrine and dopamine and used as symptomatic treatment of chorea associated with Huntington's disease but suffers from many drawbacks. Following the oral administration of tetrabenazine, the extent of absorption is found at least 75%. After single oral dose plasma concentrations of tetrabenazine are generally below the limit of detection because of the rapid and extensive hepatic metabolism of tetrabenazine (carbonyl reductase in the liver is responsible for the metabolism of tetrabenazine). This explains the need for large doses of tetrabenazine in the treatment of Huntington's disease [14]. Hence, nanocarriers applying to L-dopa, curcumin and tetrabenazine would carry optimum amount of the drug to their site of action bypassing all the barriers such as acidic pH of stomach, liver metabolism and increase the prolonged circulation of the drug into the blood due to their small size. So for delivery of the selected drugs a nano delivery system must have the following properties (i) to improve the solubility; (ii) to enhance the bioavailability; (iii) to reduce the dose; (iv) to target the site of action and (v) to control the release of the drug.

The present study primarily focuses on the design and synthesis of amphiphilic peptide sequences incorporating β-alanine and ornithine (Fig. 2), with the objective of exploring their potential utility in drug delivery applications. The selection of ornithine was based on several factors that made these systems interesting for further investigation. Ornithine is a synthetic amino acid that closely resembles lysine, with the exception of having a one-carbon shorter side-chain. Synthetic amino acids are known for their enzymatic stability, which is desirable in peptide sequences used for drug delivery systems. Therefore,

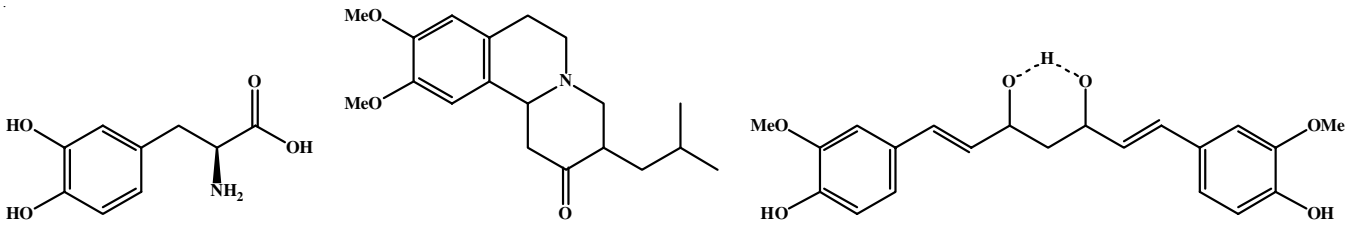

Fig. 1. Chemical structure of drugs

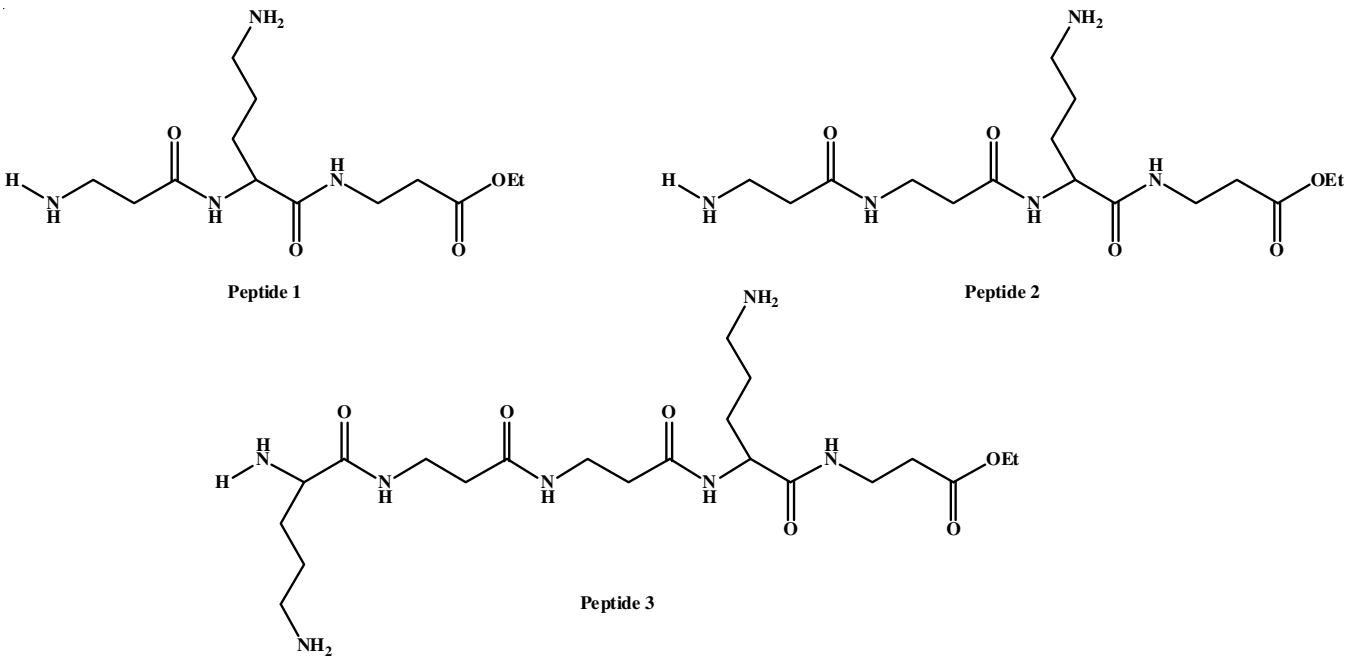

Fig. 2. Chemical structure of peptides

the inclusion of ornithine in the peptide sequences was considered suitable for this purpose. Additionally, incorporating ornithine into the peptide sequences provided a cationic charge. This cationic property is useful in biological applications because it facilitates interactions with negatively charged substances like cell membranes or drugs. Based on these considerations, the authors successfully formed self-assemblies using tri-, tetra- and penta-peptides containing β-alanine and ornithine. These self-assemblies have the potential to form nanostructures that can encapsulate drugs for delivery purposes.

EXPERIMENTAL

Boc-βAla-OEt.HCl and Boc-Orn(Z)-OH were obtained from GL Biochem Ltd., Shanghai, China. The anti-Huntington's drug tetrabenazine was obtained from TCI Chemicals Pvt. Ltd., India. Curcumin was purchased form Sigma-Aldrich Chemical Co., USA. Anti-Parkinson's drug L-Dopa was purchased from SRL Pvt. Ltd., India. Spectra/por dialysis membrane (MWCO 100-500 Da) was obtained from Spectrum Labs, USA. The spectroscopic grade solvents *viz*. tetrahydrofuran (THF), diethylether (DEE), ethyl acetate and methanol were procured from Fischer-Scientific, while trifluoroethanol (TFE) was purchased from Spectrochem Pvt. Ltd. Reagents for synthesis (puriss grade): Boc reagent, N-methylmorpholine (NMM) and trifluoroaceticacid (TFA) were obtained from Spectrochem Pvt. Ltd. and isobutylchloroformate (IBCF) was obtained from TCI Chemicals Pvt. Ltd., India.

Synthesis of peptide: The peptides were synthesized in a series by solution phase mixed anhydride method as shown in **Scheme-I**. In brief, Boc-Orn(Z)-OH (**1**) and H-βAla-OEt·HCl (**2**) were coupled using isobutylchloroformate (IBCF) and NMM as base in dry THF to obtain the Boc-Orn(Z)-βAla-OEt (**3**) with ~ 93.5 % yield. Then, Boc-group was removed from (**3**) to obtain H-Orn(Z)-βAla-OEt (**4**) which coupled with Boc-βAla-OH (**5**) and obtained Boc-βAla-Orn(Z)-βAla-OEt (**6**)

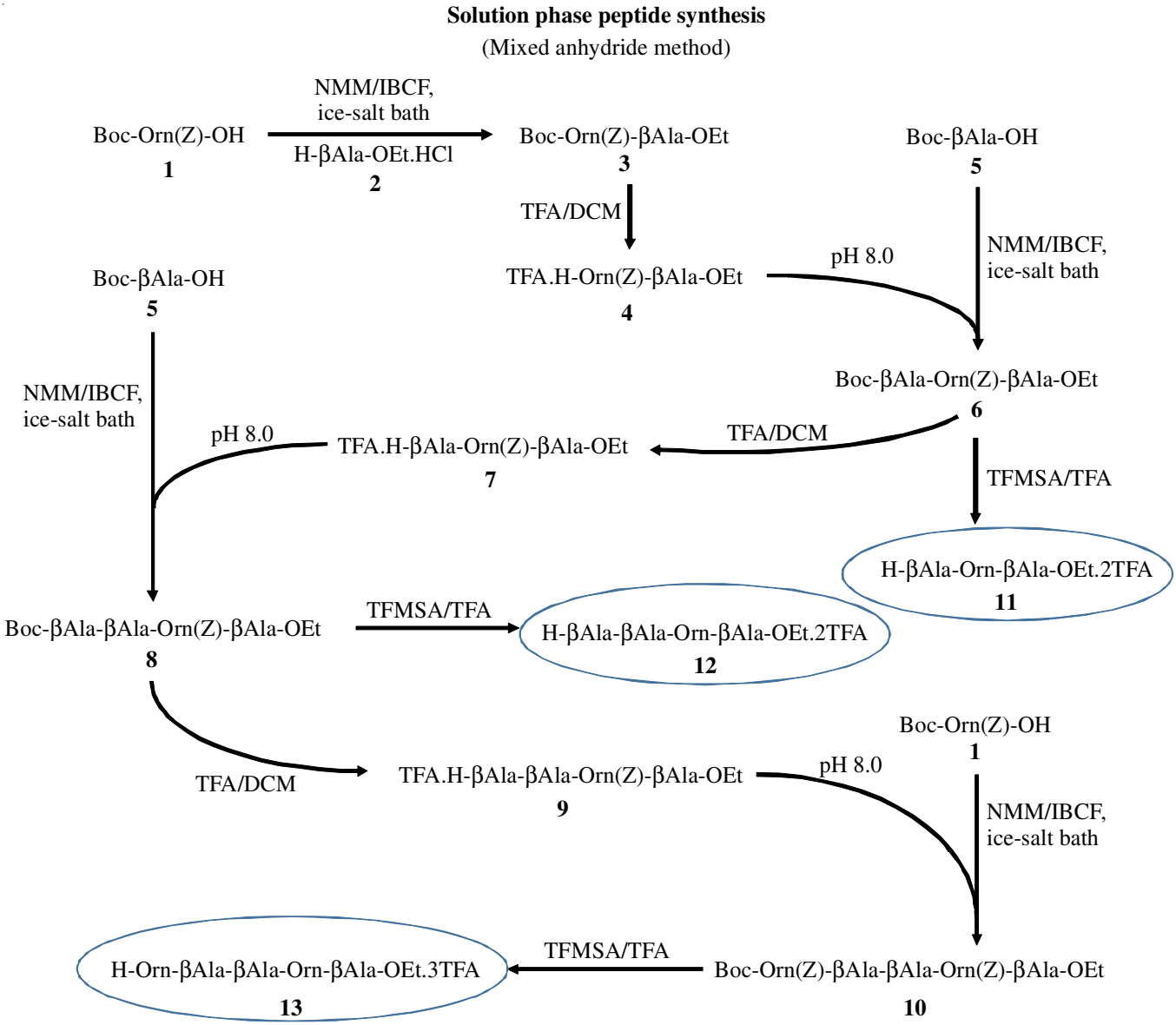

Scheme-I: Solution-phase synthesis of peptides using mixed anhydride method

with ~ 94.4 % yield. Similarly, Boc-βAla-βAla-Orn(Z)-βAla-OEt (**8**) was synthesized (83.9% yield) by removing Boc-group from Boc-βAla-Orn(Z)-βAla-OEt (**6**) to obtain H-βAla-Orn(Z)-βAla-OEt (**7**) followed by coupling with Boc-βAla-OH (**5**).

Boc-Orn(Z)-βAla-βAla-Orn(Z)-βAla-OEt (**10**) was synthesized in ~ 95.5% yield by removing Boc-group from Boc-βAla-βAla-Orn(Z)-βAla-OEt (**8**) to obtain H-Orn(Z)-βAla-Orn(Z)-βAla-OEt (**9**) followed by coupling with Boc-Orn(Z)-OH (**1**). The required peptides were obtained by removing Boc- and Z group using TFA:TFMSA from **6**, **8** and **10** to obtain H-βAla-Orn-βAla-OEt (**11**), H-βAla-βAla-Orn-βAla-OEt (**12**) and H-Orn-βAla-βAla-Orn-βAla-OEt (**13**), respectively.

Tripeptide **11**, tetrapeptide **12** and pentapeptide **13** were finally purified on RP-HPLC and characterized by mass spectrometry. The LC/ESI-MS: $[M + 2H]_{Tripeptide}$ = 304.5 (calcd. 304.5), $[M + 2H]_{Tetrapeptide}$ = 375.5 (calcd. 375.5) and $[M]_{Pentapeptide}$ = 487.5 (calculated 487.5) and $[M + H]_{Pentapeptide}$ = 488.5 (calcd. 488.5).

Preparation of self-assemblies: Peptide nanostructures was prepared by self-assembly. In brief, peptide (1 mg) was first dissolved in 100 µL methanol and then diluted with 900 µL water followed by vortexing for 2 min. After an aging of 2 h, the samples were characterized by DLS and TEM studies.

Dynamic light scattering (DLS) analysis: The size distribution and zeta potential measurements of the self-assembled unloaded peptide nanostructures and L-dopa, curcumin and tetrabenazine loaded peptide nanostructures were recorded in triplicate by dynamic light scattering (DLS) using Zetasizer Nano-ZS, Malvern Instruments.

High resolution-transmission electron microscopy (HR-TEM) analysis: Transmission electron microscopic (TEM) images were recorded using a TECNAI G^2 20 TWIN electron microscope at an accelerating voltage of 200 kV. For sampling, a drop of self-assembled peptide solution was mounted on a 200 mesh carbon coated copper grid and stained negatively with aqueous solution of 1% uranyl acetate.

Spectroscopic characterization: A Perkin-Elmer FT-IR spectrometer was used for obtaining the FT-IR spectra of samples in solid and in solution state at room temperature. For solid state, sample was prepared as a KBr disk while to obtain spectra in solution phase a methanolic solution of peptide was used in attenuated total reflectance (ATR) mode. The far-UV CD spectra were recorded at room temperature on a JASCO J-815 CD spectrometer using a quartz cell of 0.1 cm optical path length. The concentration of peptide was kept 1 mg/mL in all cases. The absorption spectra were recorded using a UV/Vis spectrophotometer (Cary Eclipse, Agilent Technologies). For peptide-drug interaction studies, the concentration of the drug solution of L-dopa, curcumin and tetrabenazine was taken 25 µg/mL, 4.6 µg/mL and 26 µg/mL, respectively, in water.

Drug-peptide interaction studies: L-Dopa, curcumin and tetrabenazine were chosen as hydrophobic molecules with maximum absorption at 280, 425 and 282 nm, respectively. Interaction study of drugs with self-assembled peptide nanoassemblies were conducted titrametrically and absorption measurements were made at each step.

Entrapment of L-dopa: L-Dopa-loaded nanostructures were prepared by dissolving peptide 5 mg in 100 µL methanol and mixed with 900 µL of L-dopa containing three different amounts 0.5 mg, 1 mg and 2 mg with continuous vortexing for 5 min. The solution was left overnight for stabilization of self-assembled nanostructures. The resulting mixture was centrifuged and the supernatant was collected and lyophilized to obtain the desired drug loaded nanostructures. Then to separate the nanostructures from excess drug, obtained nanostructures was re-dissolved in water (pure aspirin is not soluble in water) and then after centrifuge for 2 min separated supernatant was collected in other Eppendorf for further lyophilization.

Entrapment of curcumin and tetrabenazine: Drug-loaded nanostructures were prepared by dissolving peptide 5 mg and drug in different amounts in 100 µL methanol with vortexing for 2 min. Then 900 µL of water was added and again vortexed for 5 min. The solution was left overnight for stabilization of self-assembled nanostructures. The resulting mixture was centrifuged (pure curcumin and tetrabenazine is not soluble in water) and the supernatant was collected and lyophilized to obtain the desired drug loaded nanostructures.

The following formulae were used for measuring the encapsulation efficiency and drug loading content in peptide nanostructures:

$$\text{Encapsulation efficiency} = \frac{\text{Amount of drug added} - \text{Amount of free drug}}{\text{Amount of drug added}} \times 100$$

$$\text{Drug loading content} = \frac{\text{Weight of the encapsulated drug in nanostructures}}{\text{Weight of nanostructures taken}} \times 100$$

Drug release study: To study the release of the drug from the nanovesicles, 5 mg drug loaded peptide nanovesicles were taken in a dialysis membrane (MWCO 100-500 Da). The membranes were placed in 50 mL centrifuge tube containing 30 mL of PBS pH 7.4 and agitated on an orbital shaker at a continuous speed of 100 rpm. The drug release was monitored using 1 mL of the sample at fixed time intervals and absorbance was read using UV-visible spectrophotometer. After every spectroscopic measurement the solutions were returned to the main bulk.

Statistical analysis: All data were expressed as means with standard deviations (mean ± SD) and the data were analyzed using one-way ANOVA with Tukey's test. Statistical significance was defined as $p < 0.05$.

RESULTS AND DISCUSSION

The self-assembly of peptide molecules in response to solvent polarity resulted in the formation of cationic nanostructures, as confirmed by DLS measurements (Table-1). The average sizes of the structures formed by peptide **1**, **2** and **3** in aqueous medium were measured as 270 nm, 273 nm and 175 nm, respectively. The surface charge potential of peptide **1**, **2** and **3** was highly positive, measuring 40 mV, 45 mV and 42 mV, respectively. In general, the hydrodynamic diameters measured by DLS are three times larger than the actual particle diameters [15,16]. Therefore, the particle diameter measurements were confirmed using TEM measurements (Fig. 3). The average sizes of the nanostructures from TEM studies were found to be 94 ± 14 nm, 17 ± 3 nm and 99 ± 31 nm for peptide **1**, **2** and **3**,

TABLE-1
DLS MEASUREMENTS OF PEPTIDE NANOSTRUCTURES

Sample	Average size (nm) ± SD	PDI ± SD	Zeta potential (mV) ± SD
H-βAla-Orn-βAla-OEt (1) (unloaded)	270.0 ± 1.838	0.068 ± 0.004	39.7 ± 0.529
H-βAla-βAla-Orn-βAla-OEt (2) (unloaded)	273.1 ± 1.443	0.073 ± 0.008	44.9 ± 1.090
H-Orn-βAla-βAla-Orn-βAla-OEt (3) (unloaded)	175.0 ± 1.739	0.045 ± 0.009	42.0 ± 0.451

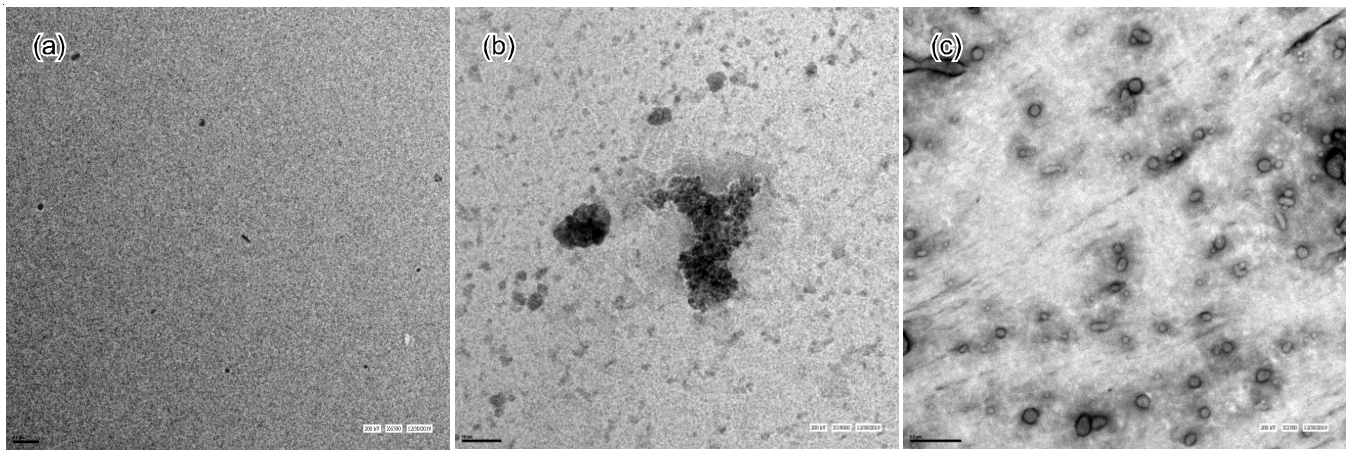

Fig. 3. TEM micrographs of (a) tripeptide 1, (b) tetrapeptide 2 and (c) pentapeptide 3 nanostructures (scale bar: (a) 100 nm, (b) 50 nm, (c) 500 nm)

respectively. In most cases, the observed morphology of peptide nanostructures was spherical. This morphology can be attributed to the hydrophobic-hydrophobic interactions among the backbone atoms, resulting in the clustering of hydrophobic regions forming the core, while the charged amino groups create the surface [17]. The TEM micrographs also displayed spherical-shaped self-assembled peptide nanostructures, confirming the findings. These results strongly indicate that the self-assembly process refines the arrangement of the peptide molecules, further enhancing their potential applications.

Secondary structure estimation: The secondary structure of the peptides was determined using circular dichroism (CD) and FTIR spectroscopic studies. The CD spectra of the peptides are shown in Fig. 4. In Fig. 4a, tripeptide exhibited a negative maximum at 195 nm in the CD spectrum. Although no positive signal crossed the zero crossing line, a positive trend in the signal was observed. A comparatively diminished positive signal at a wavelength of 214 nm was observed in 100% methanol, which is an entirely organic solvent, in contrast to the tripeptide's positive signal at 216 nm in 50% methanol and at 218 nm in 10% methanol. The negative maximum of tripeptide and the red shift from 214 nm (100% methanol) to 218 nm (10% methanol) were attributed to the effects of the chiral α-carbon of ornithine. The wavelength shift indicated that a π-π* transition was responsible for this change [18]. The spectra clearly indicated a random conformation in the tripeptide. In Fig. 4b, the tetrapeptide displayed a strong negative signal at 202 nm in 100% methanol, indicating an helical structure. In 50% methanol, the helical structure of the peptide was preserved with a slight blue shift in the negative maximum at 201 nm. The intensity of the signal decreased, suggesting a decreased population of helical conformers. However, in 10% methanol, a total loss of the helical structure was observed [19].

The tetrapeptide was unable to maintain its helical conformation in 10% methanol or aqueous solution and a random structure was observed from the recorded spectrum. Fig. 4c

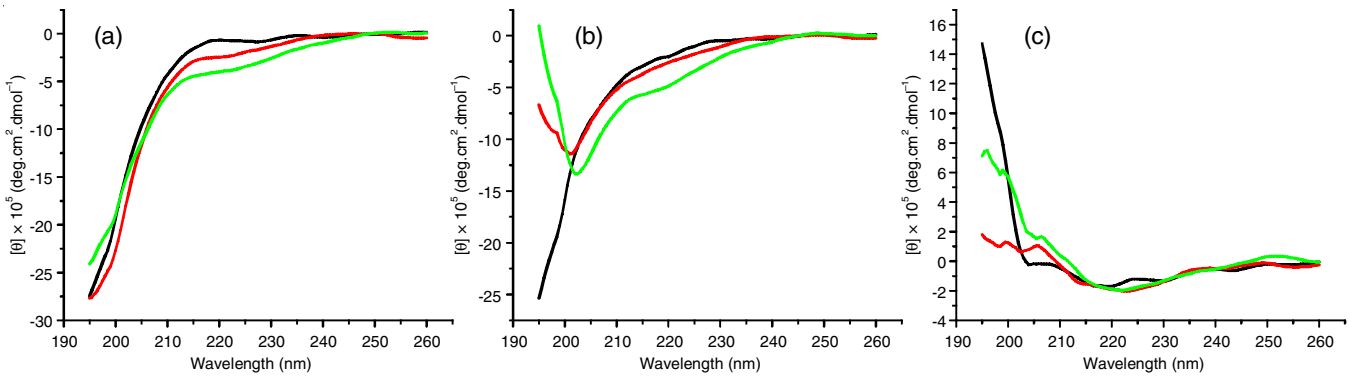

Fig. 4. CD spectra of (a) tripeptide 1, (b) tetrapeptide 2 and (c) pentapeptide 3 in 10% methanol (black), 50% methanol (red) and 100% methanol (green)

displays the CD spectra of the pentapeptide. In a 10% methanol solution, a reciprocal ellipticity was recorded compared to the tetrapeptide. The positive maximum at 195 nm indicated the helical structure of the pentapeptide in 10% methanol. Surprisingly, it was observed that pentapeptide in 100% methanol exhibited a sheet-like structure [15]. The transition from helical to sheet-like conformation was further studied and in 50% methanol, a random structure was observed.

The conformation of the peptides was also investigated using FTIR. The FTIR spectra of all the peptides were recorded in KBr (Fig 5a) and in methanol (Fig. 5b). It was observed that the spectra of all the peptides in KBr were almost similar. The major peaks at 1651, 1537 and 1223 cm^{-1} corresponded to the amide I, amide II and amide III regions, respectively. These spectral peaks indicated a random conformation of the peptides in the solid state [17]. Similarly, in methanol, the peptides exhibited a similar pattern. In methanol solution, a major peak in the amide-I region disappeared compared to the solid state. Two prominent peaks appeared, one at 1412 cm^{-1} in the amide II region and the other at 1250 cm^{-1} in the amide-III region. A strong and broad peak at 3320 cm^{-1} in methanol indicated the presence of intramolecular hydrogen bonds in the soluble state of the peptides [15,20]. The precise structural details of these β-peptide designs are yet unknown; nevertheless, the present studies indicate that the peptides adopt a folded-conformation.

Drug-peptide interaction studies: The loading of drugs into nanostructures is of paramount importance for their development as effective delivery vehicles. However, prior to drug loading, the preformed peptide nanostructures were tested for their binding affinity with drug molecules. The quantitative analysis of the intermolecular interactions was performed using a supramolecular titration method. In this method, one component (guest molecules, *i.e.*, the peptide nanostructures) was gradually added to the system (host molecules, *i.e.* the drug solution), while monitoring the absorption band (UV) at regular intervals. The resulting data was compared and fitted to binding models to obtain information such as the association constant (K_a), which provides insights into the strength of the drug-peptide interaction. Fig. 6 illustrates the interaction of L-dopa (λ_{max}: 280 nm), curcumin (λ_{max}: 425 nm) and tetrabenazine (λ_{max}: 282 nm) with the self-assembled peptide nanostructures (guest molecules). The UV spectra of the drugs were monitored during the titration process to observe any changes in the absorption bands, indicating their binding to the peptide nanostructures.

During the experiment, it was observed that the gradual addition of self-assembled peptide nanostructures to the L-dopa drug solution (in volumes of 1 µL, 2 µL, 3 µL, 4 µL, 5 µL, 10 µL, 20 µL and 100 µL) did not cause significant changes in the absorbance of the drug solution for peptides **1** and **2** (Fig. 6a-b). However, when 100 µL of peptide **3** nanostructures was added, a sharp change in the absorbance of the drug at 280 nm was observed (Fig. 6c). Additionally, a distinct change in one of the spectra was observed. In case of peptides **1** and **2**, the addition of peptide nanostructures to the drug solution resulted in a slight decrease in absorbance, whereas for peptide **3**, the absorbance increased. This suggests an association between the drug molecules and the peptide **3** assemblies [17]. Furthermore, it was observed that for peptides **1** and **2**, the spectra obtained matched exactly with those shown in Fig. 6a-b, indicating a slight decrease in absorbance at 282 nm. However, when 100 µL of peptide nanostructures was added, a significant decrease in the spectra was observed.

In case of peptide **3**, the pattern of change in absorbance intensity was reversed compared to peptides **1** and **2**. This means that the absorbance appeared to slightly increase upon addition of peptide nanostructures and for 100 µL, it showed a significant increase. For drug curcumin, a similar pattern of absorbance change was observed for all the peptides (Fig. 6d-f). The absorbance of curcumin decreased at 425 nm in all cases. However, due to the high hydrophobicity of curcumin, its binding with the peptide molecules was found to be challenging [17]. The results obtained with the drug tetrabenazine were highly interesting and informative. When the self-assembled peptide nanostructures were added to the tetrabenazine drug

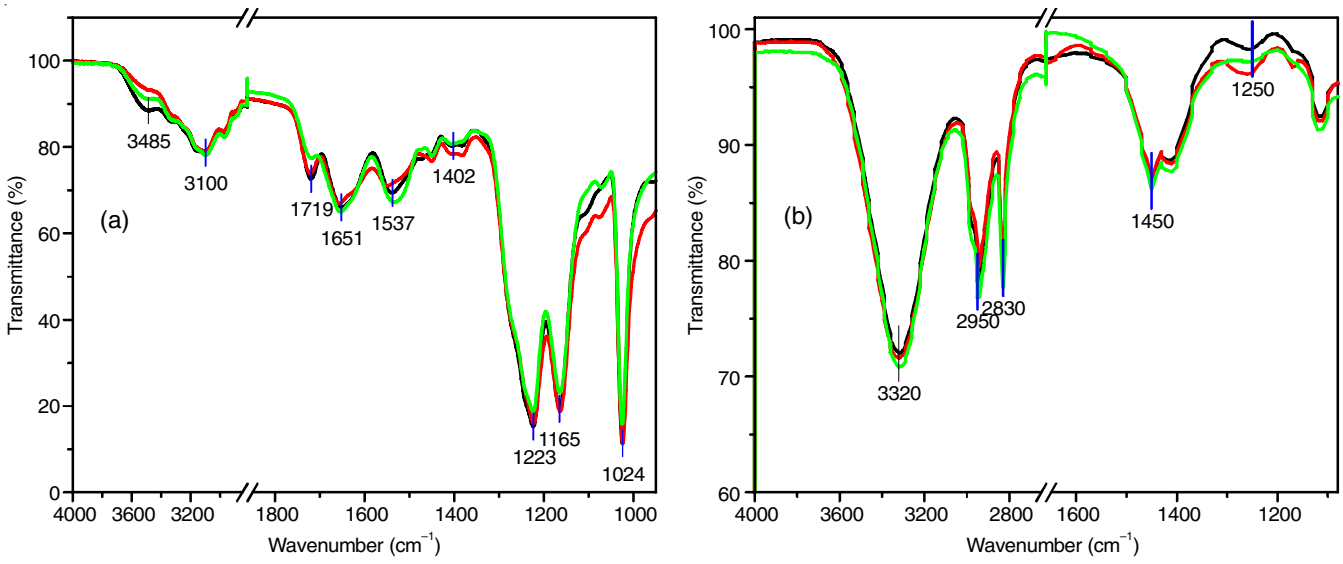

Fig. 5. FTIR spectra of tripeptide 1 (black), tetrapeptide 2 (red) and pentapeptide 3 (green) nanostructures in (a) KBr and (b) methanol

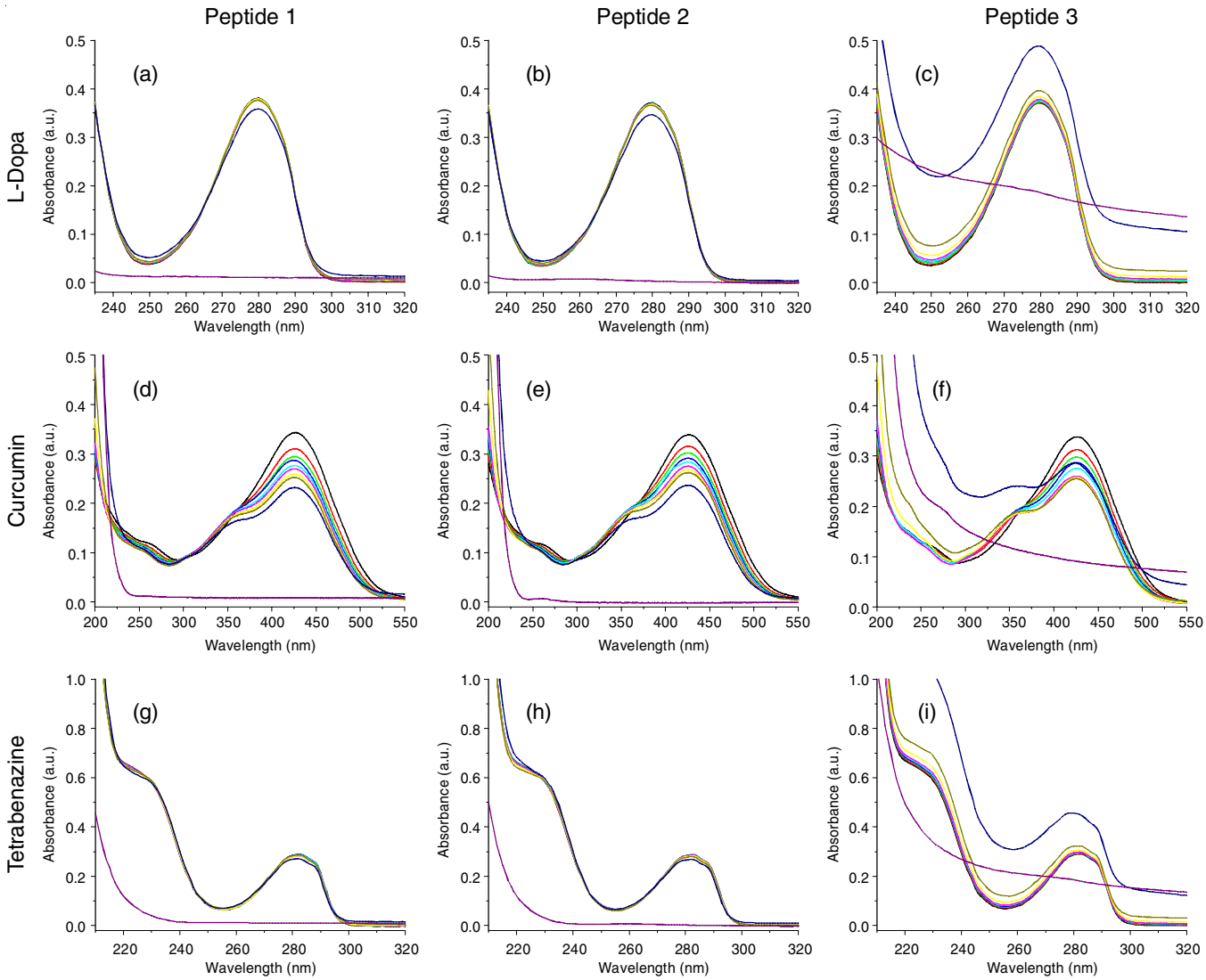

Fig. 6. UV-Vis spectra showing interaction of peptides with drug moieties L-dopa, curcumin and tetrabenazine

solution, no significant changes occurred in the absorbance of the drug solution at 282 nm. However, similar patterns of spectra were obtained for peptides **1** and **2**, as shown in Fig. 6g-h, depicting a slight decrease in absorbance at 282 nm. When 100 µL of peptide nanostructures was added, a significant decrease in absorbance was observed. On the other hand, for peptide **3**, the pattern of change in absorbance intensity was reversed, indicating a slight increase and for 100 µL, it exhibited a highly increased absorbance (Fig. 6i). This anomalous UV behaviour of tetrabenazine upon interaction with peptide **3** nanostructures strongly suggests the formation of peptide-drug conjugates [20].

The strength of the interaction between drug molecules and self-assembled peptide molecules was assessed by determining the binding constant (K_α). The calculation of the binding constant was performed using the Benesi-Hildebrand equation:

$$\frac{1}{(A - A_o)} = \frac{1}{K_a(A_{max} - A_o)[Guest]_n} + \frac{1}{[A_{max} - A_o]}$$

In present case, A_o is the absorbance of drug in question at its λ_{max} in the absence of peptide nanostructures (guest), A is the absorbance recorded in the presence of added nanostructures (A_{max}) is absorbance in presence of nanostructures at its λ_{max} and K_a is the association constant (M^{-1}). The value of K_a was calculated from the slope of the straight line plot of $1/(A\text{-}A_o)$ against $1/[Guest]_n$. The binding constant values, obtained through the UV-Vis titration method, for the drugs L-dopa, curcumin and tetrabenazine with the peptide nanostructures, are summarized in Table-2. These binding constant values were then compared to evaluate the strength of the interactions between the drugs and the peptide nanostructures [17]. By applying the Benesi-Hildebrand equation to the absorption spectra, the researchers were able to determine the binding constant, which provides information about the strength of the interaction between the drug and peptide molecules. This analysis helps in understanding the affinity and potential stability of the drug-peptide complex, which is crucial for the drug delivery applications.

Encapsulation studies: The encapsulation of drug molecules was quantified using UV-visible spectroscopy and the results were expressed as encapsulation efficiency (%). To achieve the highest encapsulation efficiency of the peptide

TABLE-2
BINDING CONSTANT ON INTERACTION OF DRUG WITH PREFORMED PEPTIDE NANOSTRUCTURES

Sample	Binding constant (M^{-1})
Ldp (1 mL, 12.68×10^{-2} mM) + peptide 1	2.64×10^5
Ldp (1 mL, 12.68×10^{-2} mM) + peptide 2	4.91×10^5
Ldp (1 mL, 12.68×10^{-2} mM) + peptide 3	8.69×10^4
Cur (1 mL, 1.25×10^{-2} mM) + peptide 1	1.16×10^5
Cur (1 mL, 1.25×10^{-2} mM) + peptide 2	8.47×10^4
Cur (1 mL, 1.25×10^{-2} mM) + peptide 3	1.17×10^5
Tbz (1 mL, 8×10^{-2} mM) + peptide 1	1.07×10^5
Tbz (1 mL, 8×10^{-2} mM) + peptide 2	2.89×10^4
Tbz (1 mL, 8×10^{-2} mM) + peptide 3	1.43×10^4

nanostructures, the drugs were encapsulated at different weight-to-weight (w/w) ratios with the peptide. For L-dopa and tetrabenazine, three different peptide:drug ratios were used: 5:0.5, 5:1 and 5:2. However, due to the highly hydrophobic nature of curcumin, it was encapsulated in the peptide at only two peptide:drug (w/w) ratios: 5:0.5 and 5:1.

The calculated encapsulation efficiencies (%) for L-dopa, curcumin and tetrabenazine are summarized in Table-3, which also additionally comprises the drug loading content, which is the amount of drug encapsulated in the vesicles as a percentage of the total vesicle weight.

The dynamic light scattering (DLS) studies were conducted subsequent to the encapsulation of hydrophobic medicinal molecules within the peptide nanostructures. The results, as shown in Table-4, indicated that compared to the unloaded particles with a size distribution of 270 nm, the size distribution of tetrabenazine-loaded nanostructures of peptide **1** increased to approximately 433 nm, with a peak intensity of 100%. Additionally, there was a significant decrease in zeta potential from 40 mV (unloaded particles) to 8 mV. For L-dopa and curcumin-loaded particles in peptide **1**, the size increased to approximately 341 nm in both cases and the zeta potential decreased to approximately 9 mV and 24 mV, respectively, compared to their respective unloaded peptide **1** nanostructures. Similarly, in peptide **2**, the average size of tetra-

TABLE-3
DRUG ENCAPSULATION STUDIES ON PEPTIDE NANOSTRUCTURES

Sample	Peptide/drug ratio	Encapsulation efficiency (%)	Drug loading content (%)
Peptide 1 (5 mg) + Ldp (0.5 mg) (4)	5:0.5	76	5
Peptide 1 (5 mg) + Ldp (1 mg) (5)	5:1	62	9
Peptide 1 (5 mg) + Ldp (2 mg) (6)	5:2	42	12
Peptide 2 (5 mg) + Ldp (0.5 mg) (7)	5:0.5	72	16
Peptide 2 (5 mg) + Ldp (1 mg) (8)	5:1	66	17
Peptide 2 (5 mg) + Ldp (2 mg) (9)	5:2	45	20
Peptide 3 (5 mg) + Ldp (0.5 mg) (10)	5:0.5	76	8
Peptide 3 (5 mg) + Ldp (1 mg) (11)	5:1	66	11
Peptide 3 (5 mg) + Ldp (2 mg) (12)	5:2	29	15
Peptide 1 (5 mg) + Cur (0.5 mg) (13)	5:0.5	2.0	0.20
Peptide 1 (5 mg) + Cur (1 mg) (14)	5:1	0.9	0.18
Peptide 2 (5 mg) + Cur (0.5 mg) (15)	5:0.5	1.8	0.20
Peptide 2 (5 mg) + Cur (1 mg) (16)	5:1	0.7	0.22
Peptide 3 (5 mg) + Cur (0.5 mg) (17)	5:0.5	1.9	0.32
Peptide 3 (5 mg) + Cur (1 mg) (18)	5:1	0.9	0.14
Peptide 1 (5 mg) + Tbz (0.5 mg) (19)	5:0.5	53	7
Peptide 1 (5 mg) + Tbz (1 mg) (20)	5:1	38	19
Peptide 1 (5 mg) + Tbz (2 mg) (21)	5:2	35	15
Peptide 2 (5 mg) + Tbz (0.5 mg) (22)	5:0.5	62	15
Peptide 2 (5 mg) + Tbz (1 mg) (23)	5:1	50	20
Peptide 2 (5 mg) + Tbz (2 mg) (24)	5:2	36	21
Peptide 3 (5 mg) + Tbz (0.5 mg) (25)	5:0.5	65	22
Peptide 3 (5 mg) + Tbz (1 mg) (26)	5:1	58	16
Peptide 3 (5 mg) + Tbz (2 mg) (27)	5:2	36	24

TABLE-4
DLS MEASUREMENTS OF DRUG ENCAPSULATED PEPTIDE NANOSTRUCTURES

Sample	Average size (nm) ± SD	PDI ± SD	Zeta potential (mV) ± SD
H-βAla-Orn-βAla-OEt (6) (loaded with Ldp)	341.4 ± 36.66	0.306 ± 0.091	8.59 ± 1.70
H-βAla-βAla-Orn-βAla-OEt (9) (loaded with Ldp)	503.8 ± 42.78	0.246 ± 0.079	14.2 ± 1.20
H-Orn-βAla-βAla-Orn-βAla-OEt (12) (loaded with Ldp)	161.9 ± 3.453	0.107 ± 0.011	41.7 ± 1.46
H-βAla-Orn-βAla-OEt (14) (loaded with Cur)	340.9 ± 8.316	0.168 ± 0.038	23.7 ± 1.31
H-βAla-Orn-βAla-OEt (16) (loaded with Cur)	437.5 ± 1.358	0.350 ± 0.044	18.1 ± 1.65
H-βAla-βAla-Orn-βAla-OEt (18) (loaded with Cur)	362.0 ± 5.116	0.369 ± 0.007	32.1 ± 0.500
H-Orn-βAla-βAla-Orn-βAla-OEt (21) (loaded with Tbz)	432.8 ± 105.4	0.458 ± 0.061	8.11 ± 0.113
H-βAla-βAla-Orn-βAla-OEt (23) (loaded with Tbz)	549.7 ± 86.59	0.279 ± 0.101	18.0 ± 0.839
H-Orn-βAla-βAla-Orn-βAla-OEt (27) (loaded with Tbz)	219.7 ± 18.46	0.319 ± 0.048	34.1 ± 1.76

benazine-loaded nanostructures increased to approximately 550 nm from 273 nm, with a significant decrease in zeta potential from 45 mV to 18 mV. In case of L-dopa and curcumin-loaded particles, the sizes increased to approximately 504 nm and 438 nm, while the zeta potentials decreased to approximately 14 mV and 18 mV, respectively, in comparison to their respective unloaded peptide **2** nanostructures. In peptide **3**, the average size of tetrabenazine-loaded nanostructures was measured at 220 nm, accompanied by a zeta potential of 34 mV. For L-dopa and curcumin-loaded nanostructures, the sizes were recorded as 162 nm and 362 nm, respectively, with zeta potentials of 42 mV and approximately 32 mV when compared to their respective unloaded peptide **3** nanostructures.

The higher hydrodynamic diameter values observed for the drug-loaded self-assembled nanostructures may be attributed to their aggregated form. However, the actual sizes of the drug-loaded self-assembled structures were determined using TEM technique (Fig. 7). In TEM analysis, the size of peptide **1** nanostructures loaded with L-dopa, curcumin and tetrabenazine were measured as 120 nm, 70 nm and 20 nm, respectively. It is evident that the average sizes of the drug-loaded peptide nanostructures were relatively small. The reduction in particle size after encapsulating hydrophobic drugs strongly suggests the presence of hydrophobic pockets within the self-assembled nanostructures. The interactions between these hydrophobic spaces and the hydrophobic moieties of the

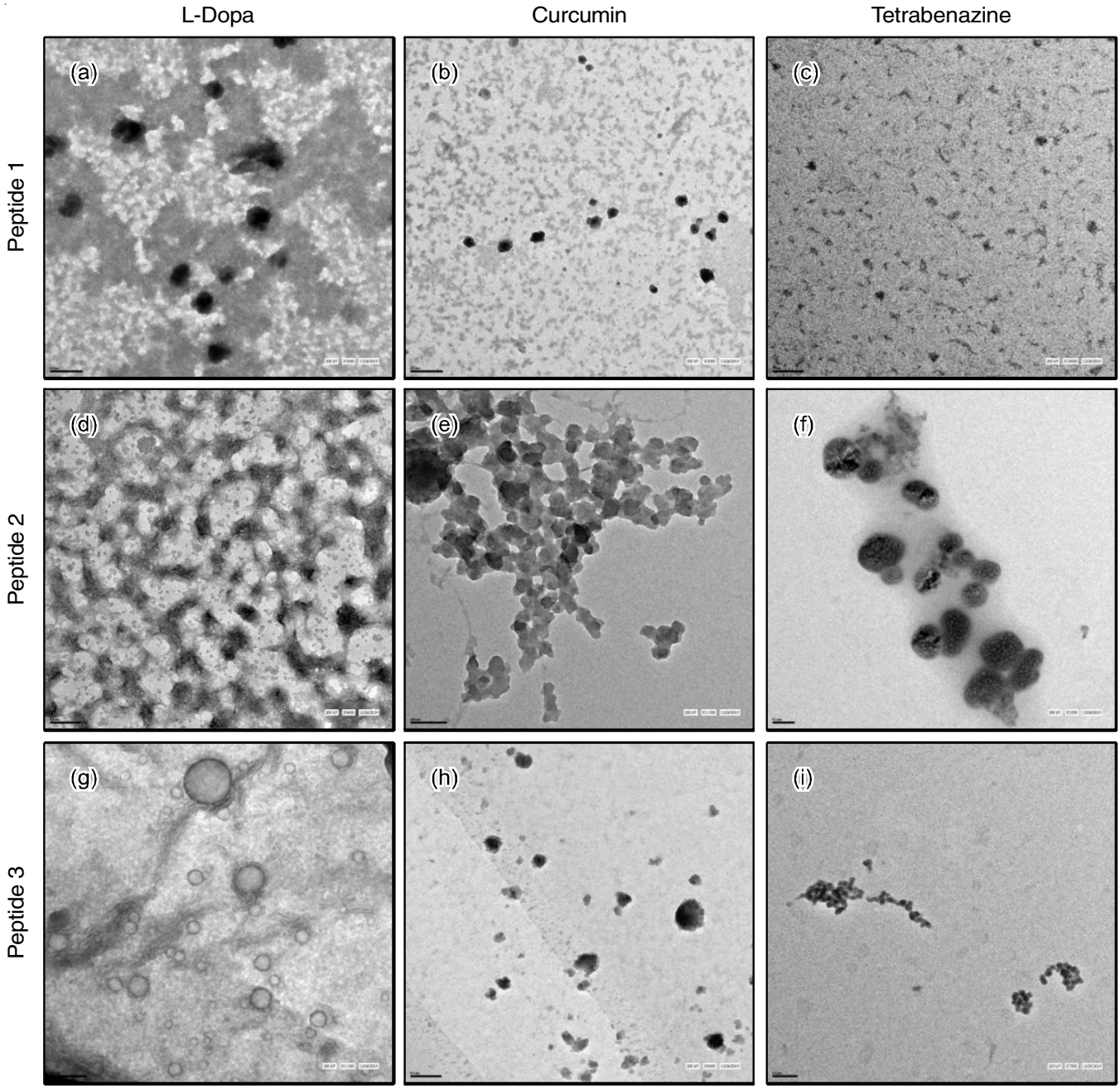

Fig. 7. TEM micrographs showing drug encapsulated nanostructures (scale bar: (a) 200 nm, (b) 200 nm, (c) 50 nm, (d) 100 nm, (e) 100 nm, (f) 200 nm, (g) 100 nm, (h) 100 nm, (i) 100 nm)

encapsulated molecules have resulted in a compact structure. Similarly, for peptide **2**, the drug-loaded nanostructures with L-dopa, curcumin and tetrabenazine exhibited sizes of 60 nm, 40 nm and 30 nm, respectively. For peptide **3**, the drug-loaded nanostructures with L-dopa, curcumin and tetrabenazine showed sizes of 40 nm, 110 nm and 25 nm, respectively. The TEM results provides the direct visualization of the drug-loaded peptide nanostructures, confirming their compact and well-defined structures.

Drug release kinetics: The *in vitro* release of the drugs from the drug-loaded nanostructures was performed using the dialysis method in 1X PBS at pH 7.4 and the release was monitored using UV-Vis spectroscopy (Table-5). The drug release kinetics of tetrabenazine were monitored for 102 h. The results indicated that peptide **1** released 17% of encapsulated drug, peptide **2** released 21% of drug, while peptide **3** released 11% of the encapsulated tetrabenazine. The percentage release *vs.* time graphs for tetrabenazine release is shown in Fig. 8c.

For curcumin, the results showed that peptide **1** released 81% of encapsulated drug within 52 h, while peptide **2** released 73% of drug in the same time frame (Fig. 8b). Peptide **3** released 91% of encapsulated curcumin within 31 h. Similarly for L-dopa, peptide **1** released 90% of encapsulated drug within 5 h, while peptide **2** and peptide **3** released 89% and 99% of encapsulated drug, respectively, within 6 h (Fig. 8a).

The release of drugs from the self-assembled nanostructures occurred in a controlled manner. Since the active molecules were physically entrapped within the hydrophobic matrix of the nanostructures, it was speculated that the release mainly occurred through diffusion. The release kinetics demonstrated efficient and slow release of tetrabenazine and curcumin from the loaded nanostructures, while L-dopa exhibited a more gradual release pattern. The DLS measurements of the peptide nanostructures after drug release were summarized in Table-6. The comparatively small sizes of peptides **1**, **2** and **3** after the release of L-dopa, along with its early release, suggest that the drug was primarily encapsulated on the surface of the nanostructures. The observed substantial enlargement of the drug (curcumin and tetrabenazine)-loaded peptide nanostructures' diameter indicates a significant change in the morphology of the nanostructures upon drug release.

Conclusion

In this study, the synthesis of an amphiphilic mixed α/β-peptide series consisting of tri-, tetra- and penta-peptides was carried out. The peptide structures were deliberately designed

TABLE-5
In vitro DRUG RELEASE KINETICS OF PEPTIDE NANOSTRUCTURES IN AQUEOUS MEDIUM

Time (h)	Peptide 1			Peptide 2			Peptide 3		
	Ldp	Cur	Tbz	Ldp	Cur	Tbz	Ldp	Cur	Tbz
1	19.5	6.6	1.5	18.6	5.5	1.8	19.2	6.8	1.7
2	34.9	7.2	2.2	33.7	10.2	3.0	40.8	12.4	2.4
3	57.1	8.0	3.2	53.4	5.9	4.1	55.3	10.2	3.0
4	72.5	7.7	3.7	66.5	6.4	5.0	69.6	12.1	3.4
5	89.5	18.2	4.0	79.3	11.3	5.8	85.0	24.4	3.6
6	–	9.9	4.5	89.0	8.7	6.5	99.0	13.6	4.0
7	–	15.0	5.1	–	12.9	7.1	–	26.3	4.4
8	–	25.7	5.1	–	11.2	7.5	–	28.5	4.6
9	–	20.5	–	–	13.0	–	–	26.9	–
23	–	14.9	8.3	–	8.8	10.5	–	40.5	5.7
24	–	24.3	7.9	–	10.5	11.9	–	24.7	6.4
25	–	14.4	–	–	11.3	–	–	22.7	–
26	–	22.0	8.3	–	15.7	12.2	–	28.7	6.5
27	–	5.2	–	–	11.2	–	–	12.5	–
28	–	26.6	8.5	–	22.9	12.4	–	38.9	6.6
29	–	21.8	–	–	18.1	–	–	47.8	–
30	–	26.9	8.6	–	24.3	12.7	–	68.6	6.8
31	–	31.2	–	–	30.2	–	–	91.1	–
32	–	–	–	–	–	–	–	–	–
47	–	–	–	–	50.1	16.3	–	–	9.7
48	–	82.0	10.9	–	57.5	16.6	–	–	9.8
50	–	–	11.2	–	–	17.0	–	–	10.1
52	–	81.1	11.6	–	72.9	17.0	–	–	10.2
54	–	–	12.1	–	–	18.0	–	–	10.4
71	–	–	12.8	–	–	18.8	–	–	10.5
72	–	–	13.0	–	–	19.0	–	–	10.7
74	–	–	13.6	–	–	19.4	–	–	10.9
76	–	–	13.8	–	–	18.8	–	–	10.6
78	–	–	14.0	–	–	18.9	–	–	10.7
96	–	–	15.7	–	–	20.1	–	–	11.0
98	–	–	17.4	–	–	23.1	–	–	11.7
100	–	–	16.1	–	–	20.5	–	–	11.2
102	–	–	16.6	–	–	21.2	–	–	11.2

TABLE-6
DLS MEASUREMENTS OF PEPTIDE NANOSTRUCTURES AFTER DRUG-RELEASE STUDIES

Sample	Average size (nm) ± SD	PDI ± SD	Zeta potential (mV) ± SD
H-βAla-Orn-βAla-OEt (28) (after release of Ldp)	177.9 ± 2.804	0.354 ± 0.036	-8.37 ± 0.278
H-βAla-βAla-Orn-βAla-OEt (29) (after release of Ldp)	229.6 ± 11.66	0.516 ± 0.042	-7.50 ± 0.197
H-Orn-βAla-βAla-Orn-βAla-OEt (30) (after release of Ldp)	389.4 ± 35.74	0.445 ± 0.366	-4.46 ± 0.347
H-βAla-Orn-βAla-OEt (31) (after release of Cur)	588.0 ± 29.66	0.260 ± 0.166	-9.87 ± 1.55
H-βAla-βAla-Orn-βAla-OEt (32) (after release of Cur)	627.6 ± 5.198	0.281 ± 0.072	-8.76 ± 0.271
H-Orn-βAla-βAla-Orn-βAla-OEt (33) (after release of Cur)	729.6 ± 31.18	0.159 ± 0.048	-5.71 ± 0.350
H-βAla-Orn-βAla-OEt (34) (after release of Tbz)	878.8 ± 30.45	0.202 ± 0.043	-5.35 ± 0.369
H-βAla-βAla-Orn-βAla-OEt (35) (after release of Tbz)	759.4 ± 23.86	0.095 ± 0.082	-4.28 ± 0.165
H-Orn-βAla-βAla-Orn-βAla-OEt (36) (after release of Tbz)	790.3 ± 36.10	0.126 ± 0.034	-7.32 ± 0.355

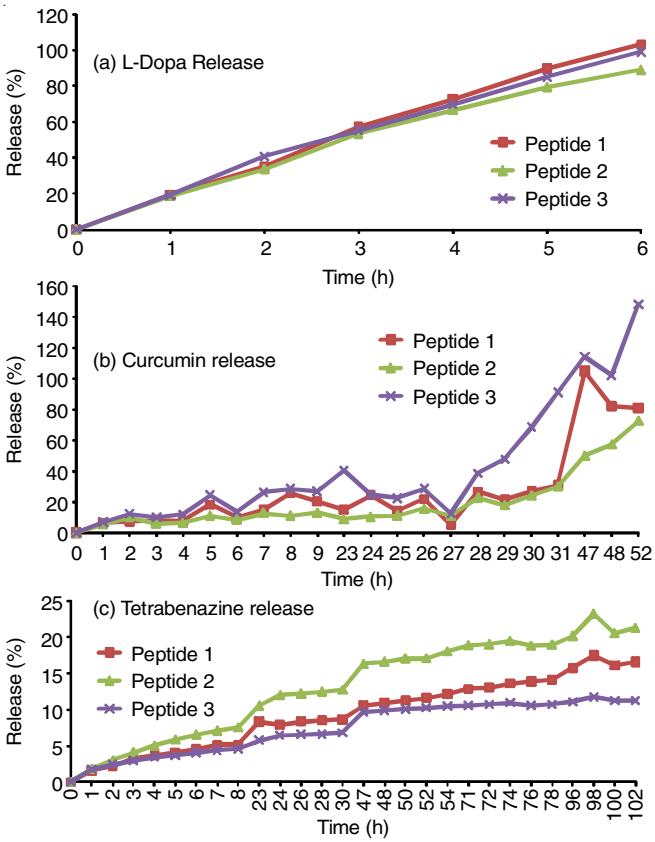

Fig. 8. Drug release profile from self-assembled drug encapsulated peptide nanostructures

to exhibit amphiphilic characteristics, rendering them well-suited for the delivery of hydrophobic pharmaceutical compounds. Present findings revealed that the nanostructures formed by peptide **2** demonstrated the highest efficiency in releasing tetrabenazine, curcumin and L-dopa. The release of tetrabenazine from both peptide nanostructures **1** and **3** exhibited similar trends. However, when it came to the release of curcumin, peptide **1** outperformed peptide **3**. On the other hand, peptide **3** showed a higher release of L-dopa compared to peptide **1**. These observations clearly indicated the capability of the designed nanostructures to effectively retain and release a significant amount of drug molecules. The results in this study emphasized the potential of these nanostructures as promising drug delivery carriers *in vitro*. The successful encapsulation and subsequent controlled release of the hydrophobic drugs demonstrate the feasibility and efficacy of the peptide-based delivery system. This study provides the foundation for further inquiries and refinement of these nanostructures in order to explore their potential applications in drug delivery and therapeutic interventions.

ACKNOWLEDGEMENTS

The authors express their gratitude to the Director, Institute of Genomics and Integrative Biology (IGIB) for providing the necessary infrastructure and facilities. The authors also extended their appreciation to the SAIF, CDRI in Lucknow for granting access to the LCMS facility, as well as the Central Facility at the North Campus of the University of Delhi for providing access to the FTIR facilities. The present research work is funded by the Council for Scientific and Industrial Research (CSIR), New Delhi, under the grant number F.No. 31/043(0390)2018-EMR-I.

CONFLICT OF INTEREST

The authors declare that there is no conflict of interests regarding the publication of this article.

REFERENCES

1. R. Huang, R. Su, W. Qi, J. Zhao and Z. He, *Nanotechnology*, **22**, 245609 (2011); https://doi.org/10.1088/0957-4484/22/24/245609
2. L.J. Németh, Z. Hegedüs and T.A. Martinek, *J. Chem. Inf. Model.*, **54**, 2776 (2014); https://doi.org/10.1021/ci5003476
3. F. d'Orlyé, L. Trapiella-Alfonso, C. Lescot, M. Pinvidic, B.-T. Doan and A. Varenne, *Molecules*, **26**, 4587 (2021); https://doi.org/10.3390/molecules26154587
4. £. Berlicki, L. Pilsl, E. Wéber, I.M. Mándity, C. Cabrele, T.A. Martinek, F. Fülöp and O. Reiser, *Angew. Chem. Int. Ed.*, **51**, 2208 (2012); https://doi.org/10.1002/anie.201107702
5. K. Kulkarni, N. Habila, M.P. Del Borgo and M.-I. Aguilar, *Front Chem.*, **7**, 70 (2019); https://doi.org/10.3389/fchem.2019.00070
6. M. Szefczyk, *Nanoscale*, **13**, 11325 (2021); https://doi.org/10.1039/D1NR02220B
7. P. Moitra, K. Kumar, P. Kondaiah and S. Bhattacharya, *Angew. Chem. Int. Ed.*, **53**, 1113 (2014); https://doi.org/10.1002/anie.201307247
8. F. Fülöp, T.A. Martinek and G.K. Tóth, *Chem. Soc. Rev.*, **35**, 323 (2006); https://doi.org/10.1039/b501173f
9. M. Yang, D. Xu, L. Jiang, L. Zhang, D. Dustin, R. Lund, L. Liu and H. Dong, *Chem. Commun.*, **50**, 4827 (2014); https://doi.org/10.1039/C4CC01568A

10. S.S. Suri, H. Fenniri and B. Singh, *J. Occup. Med. Toxicol.*, **2**, 16 (2007); https://doi.org/10.1186/1745-6673-2-16
11. N. Ngwuluka, V. Pillay, L.C. Du Toit, V. Ndesendo, Y. Choonara, G. Modi and D. Naidoo, *Expert Opin. Drug Deliv.*, **7**, 203 (2010); https://doi.org/10.1517/17425240903483166
12. M.S. Gunay, A.Y. Ozer and S. Chalon, *Curr. Neuropharmacol.*, **14**, 376 (2016); https://doi.org/10.2174/1570159X14666151230124904
13. S. Dhivya and A. Rajalakshmi, *PharmaTutor*, **5**, 30 (2017).
14. N. Kaur, P. Kumar, S. Jamwal, R. Deshmukh and V. Gauttam, *Ann. Neurosci.*, **23**, 176 (2016); https://doi.org/10.1159/000449184
15. R. Goel, A.K. Sharma and A. Gupta, *New J. Chem.*, **41**, 2340 (2017); https://doi.org/10.1039/C6NJ03281H
16. M. Mahato, V. Arora, R. Pathak, H.K. Gautam and A.K. Sharma, *Mol. Biosyst.*, **8**, 1742 (2012); https://doi.org/10.1039/c2mb25023c
17. R. Goel, C. Garg, H.K. Gautam, A.K. Sharma, P. Kumar and A. Gupta, *Int. J. Biol. Macromol.*, **111**, 880 (2018); https://doi.org/10.1016/j.ijbiomac.2018.01.079
18. C.A. Olsen, M. Lambert, M. Witt, H. Franzyk and J.W. Jaroszewski, *Amino Acids*, **34**, 465 (2008); https://doi.org/10.1007/s00726-007-0546-8
19. D.H. Appella, J.J. Barchi, S.R. Durell and S.H. Gellman, *J. Am. Chem. Soc.*, **121**, 2309 (1999); https://doi.org/10.1021/ja983918n
20. R. Goel, S. Gopal and A. Gupta, *J. Mater. Chem. B Mater. Biol. Med.*, **3**, 5849 (2015); https://doi.org/10.1039/C5TB00652J